Original paper

Cytotoxicity of gold nanoparticles to human lymphocytes: a comparison between rod-shaped and spherical nanoparticles

Jacek Sikora[1], Paulina Błaszkiewicz[2], Alina Dudkowiak[2], Joanna Jagielska[3], Jakub Żurawski[1]

[1]Department of Immunobiology, Poznan University of Medical Sciences, Poznan, Poland
[2]Faculty of Materials Engineering and Technical Physics, Poznan University of Technology, Poznan, Poland
[3]Department of Bioinformatics and Computational Biology, Poznan University of Medical Sciences, Poznan, Poland

Introduction: Gold nanoparticles (AuNPs) have unique properties that promise new and improved methods for targeting cancer treatment and diagnosis. However, despite their relatively high biocompatibility, AuNPs can negatively affect cell viability. Research indicates that the interactions with the plasma membrane and cellular uptake of AuNPs depend significantly on size, shape, and surface modifications.

Material and methods: We evaluated the use of human lymphocyte primary culture as a model for assessing the toxicity of AuNPs in proliferating cells. We compared the toxicity of rod-shaped, PEGylated AuNPs (gold nanorods, AuNRs) of two different sizes and gold nanospheres (AuNSs).

Results: Our results show that at high concentrations, both AuNSs and AuNRs negatively affect the viability of activated human lymphocytes *in vitro*. The cytotoxic effect varies with size and concentration, with larger AuNRs (approx. 22 × 50 nm) being more toxic than smaller ones (approx. 20 × 40 nm) and 15 nm AuNSs exhibiting the lowest toxicity.

Conclusions: Our results confirm that the application of AuNPs in cancer therapy and diagnostics must be accompanied by a thorough cytotoxicity assessment. Despite certain limitations, using the 3-(4,5-dimethylthiazol-2-yl)-2,5-diphenyltetrazolium bromide (MTT) reduction test for viability assessment of proliferating cells proves to be a simple and cost-effective method useful in nanoparticle toxicity studies.

Key words: gold nanoparticles, gold nanorods, immunotoxicity, lymphocytes, nanomaterials, toxicity, theranostic nanoparticles.

Contemp Oncol (Pozn) 2024; 28 (4): 326–334
DOI: https://doi.org/10.5114/wo.2024.146995

Introduction

Gold nanoparticles (AuNPs), due to their relatively low toxicity and unique, tunable optical properties, are promising candidates for many cancer treatment and diagnostic applications, ranging from medical imaging and drug delivery to light-activated therapies [1]. Apart from their distinctive chemical and physical characteristics and their ease of synthesis in various shapes and sizes, low toxicity is a key factor driving the significant interest in AuNPs. Among the various morphologies, gold nanospheres (AuNSs) of different sizes and rod-shaped nanoparticles (AuNRs) of various sizes and aspect ratios (ARs) have been studied the most extensively [2]. Gold in the form of a colloidal suspension of nanoparticles exhibits high biocompatibility due to its high chemical and physical stability. The negative surface charge on AuNPs facilitates the conjugation of various functional groups, ligands, or other biomolecules and chemicals, including drugs, nucleic acids, and antibodies [3, 4].

The localized surface plasmon resonance band (LSPR) of AuNPs is widely recognized for its coherent oscillations of conduction band electrons on the AuNP surface upon light excitation. The wavelength of the LSPR band is determined by the chemical structure, size, shape, and clustering of the AuNPs [5]. Many biological detection and imaging methods utilize the LSPR bands of AuNPs. In particular, AuNRs are excellent candidates as light absorbers, enabling the selective elimination of tumor cells in photodynamic and photothermal therapies [6]. In photodynamic therapy, AuNRs with suitable properties, when taken up by target cells, facilitate the local generation of reactive oxygen species in tissues irradiated with laser light of an appropriate wavelength within the visible or infrared range [7]. In the photothermal approach, abnormal cells are eliminated through a local temperature increase in cells that internalize light-absorbing AuNPs [8–10].

Further research is needed on the metabolism of gold in living organisms. Therapies using this metal require a thorough evaluation of their efficacy. It would also be desirable to develop a form of gold that can be fully metabolized. The shape and morphology of AuNPs impact their biodistribution and circulation in the body. To ensure the safe utilization of AuNPs in clinical practice, it is necessary to improve pharmacokinetics and targeting efficacy and to determine delayed toxicity [11].

AuNPs intended for biomedical applications require functionalization to prevent aggregation and deposition while maintaining their plasmonic functionalities. Naked (nonstabilized), uncharged nanoparticles lose their colloidal stability and tend to aggregate. Aggregated nanoparticles not only

lose their plasmonic functionalities but also undergo rapid clearance by the mononuclear phagocyte system (MPS), making them susceptible to being trapped in narrow capillary beds and reducing their total circulation time [12]. A frequently used method for stabilizing AuNPs is coating their surface with polyethylene glycol (PEG) [13] PEGylation prevents the adsorption of surface proteins in biological media [14], reduces clearance by the MPS, and prevents cellular uptake [15].

It has been repeatedly shown that, apart from light-activated effects exploited in cancer therapy, AuNPs alone, despite generally high biocompatibility, negatively affect cell viability [16]. Adverse effects on cells were observed for both naked and PEGylated AuNPs [17]. AuNPs induce the production of reactive oxygen species, reduce the potential of the mitochondrial membrane, and, consequently, induce autophagy, apoptosis, or necrosis [18–20]. The cytotoxicity of AuNPs depends on factors such as concentration, size, shape, surface area, surface charge, capping (stabilizing) agent, and roughness [21]. It is also influenced by the properties of the medium in which the particles are suspended. The presence of serum proteins forming the protein corona alters the physicochemical characteristics of AuNPs and affects the results of *in vitro* tests [14, 22].

The size and AR of AuNRs are key parameters that determine their optical properties and interactions with cells. Cellular uptake, retention, and distribution within the cell are highly dependent on the size and dimensions of AuNRs [23, 24]. Both theoretical modeling and experimental studies demonstrate that the toxicity of nanoparticles, which is partly dependent on cellular uptake, is related to the size and shape of the AuNPs.

Computational modeling of nanoparticle-membrane interactions shows that AR affects the rate of AuNP internalization [25, 26]. Experimental evidence demonstrates that cylindrical nanoparticles with a high AR are more efficiently captured by cells due to a greater adhesion force between the cell membrane and the nanoparticle surface [27–29]. However, some experimental studies report conflicting results. In a study on the uptake of citric acid-stabilized AuNSs (AR = 1 : 1), Chithrani *et al*. [24] found that AuNSs (with diameters of 14 and 74 nm ± 10%) were more readily internalized by HeLa cells than AuNRs (14 × 40 and 14 × 74 ± 10%). Other studies have found a non-linear relationship between dimensions and AuNP internalization. For instance, the cellular uptake of non-PEGylated AuNPs by prostate cancer cells (PC-3) is higher for 50-nm AuNSs than for AuNRs in the size range of 30 to 90 nm [30]. There is an optimal particle size for the most efficient membrane wrapping in receptor-mediated endocytosis, one of the mechanisms of AuNP internalization [26, 31, 32].

The relationship between AuNP internalization and toxicity is also complex. Smaller AuNSs can enter the nucleus, whereas larger ones tend to accumulate in the cytoplasm [33, 34]. Nuclear localization is usually associated with higher toxicity [35]. Studies have shown that non-PEGylated AuNSs exhibit significant toxicity *in vivo* only within a certain diameter range (8–37 nm) [36]. An inverse correlation between cellular uptake and AR was found for cetyltrimethylammonium bromide (CTAB)-coated AuNRs with a length range of 33 to 55 nm and ARs from 1.1 to 4.0 in MCF-7 cells, although no association of AR with cell viability was observed. Instead, the observed cytotoxic effect could be attributed to CTAB molecules in the nanoparticle suspension [37].

Kinnear *et al*. [38] suggested that the effect of AR on cellular uptake may be overestimated. The synthesis of AuNPs of different dimensions requires different chemical environments, resulting in nonidentical chemical composition of the final AuNP suspensions. To ensure consistent chemical compositions of the AuNP suspensions, the team used the thermal reshaping method to obtain different ARs from a single batch of AuNPs. Experiments involving AuNPs functionalized with polyvinylpyrrolidone (PVP) and epithelial-derived cells (A549, HeLa), as well as macrophages (J774A.1), have shown that once variables other than AR were eliminated, there was minimal to no effect of AR on AuNP uptake. The analysis of the size- and shape-dependent cytotoxicity of AuNPs is important in the context of their potential applications, mainly because the size of the AuNPs affects their biodistribution *in vivo* [39]. Because intravenous injection is the typical route of administration for biomedical AuNPs, understanding the interactions between AuNPs and circulating cells of the immune system is essential.

Here, we present the results of the viability evaluation of activated human peripheral blood lymphocytes exposed to PEGylated AuNSs and AuNRs of two different sizes. Activated lymphocytes were chosen as a model of carcinogenesis due to their metabolic similarities with proliferating cancer cells [40]. Lymphocyte viability was assessed after activation with phytohemagglutinin (PHA-L), a potent mitogen that binds nonspecifically to T-cell receptors and stimulates cytokine production and secretion, expression of surface molecules, and cell proliferation.

Material and methods

Chemicals

Tetrachloroauric acid ($HAuCl_4 \cdot H_2O$) (with a purity of 99.99%) was purchased from Alfa Aesar (USA), and sodium citrate ($HOC(COONa)(CH_2COONa)_2 \cdot 2H_2O$) (≥ 99.00%), CTAB (99.00%), sodium borohydride ($NaBH_4$) (98.00%), silver nitrate ($AgNO_3$) (99.99%), ascorbic acid (AA) (99.00%), O-(2-mercaptoethyl)-O'-methylpolyethylene glycol (PEG-SH Mw ≈ 2000) (99.99%), and saline solution were purchased from Sigma-Aldrich (USA).

Chemical synthesis of AuNPs

All chemicals were dissolved in ultrapure Milli-Q water (18.2 MΩ·cm, 71.98 ± 0.01 $mN \cdot m^{-1}$) in glass flasks treated with aqua regia before use. Gold nanospheres (AuNSs) were obtained in one-step bottom-up *in situ* reactions, using $HAuCl_4$ as the precursor and sodium citrate as the reducer [41, 42]. Sodium citrate was used to reduce the aqueous $HAuCl_4$ solution. Sodium citrate cannot reduce $HAuCl_4$ to metallic gold when the reaction solution is cold; the reaction takes place only when heated. For this purpose, 17.623 ml of a 1% $HAuCl_4$ aqueous solution was dissolved in 500 ml of Milli-Q water. The solution was then placed

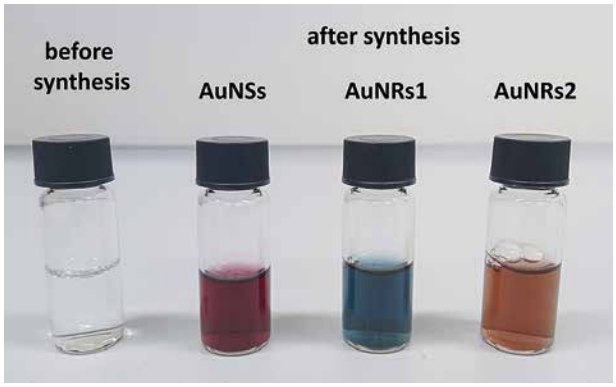

Fig. 1. Color change determined by the shape and size of the nanoparticles

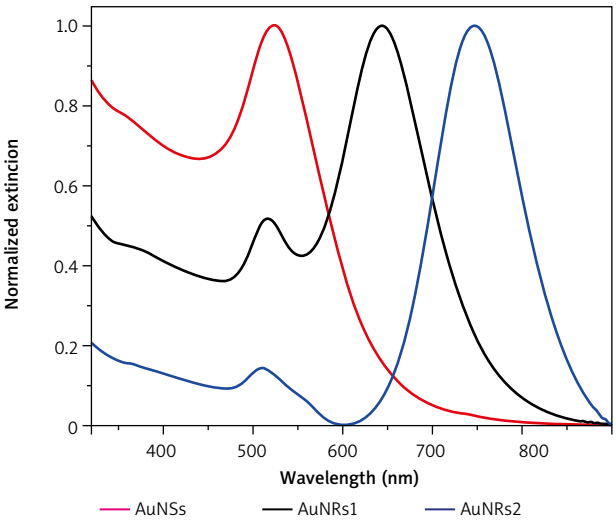

Fig. 2. Normalized extinction spectra of spherical gold nanospheres (AuNSs, red) and gold nanorods (AuNRs) with varying concentrations of $AgNO_3$ in the growth solution: 0.075 ml (AuNRs1, black) and 0.25 ml (AuNRs2, blue)

on a heating plate and brought to a boil with stirring (temperature on the heat plate approx. 170°C). Next, 596.6 mg of sodium citrate was dispersed in 51.762 ml of water and rapidly added with vigorous stirring. The solution should change color from clear to yellow to dark red (Fig. 1). After adding sodium citrate, the solution was stirred and heated (approx. 170°C) for 45 min. Once the heat was removed, the solution continued to be stirred while cooling to room temperature. The reaction mixture then took on the characteristic color of AuNSs. Subsequently, the solution was filtered through syringe filters (22 µm) [41, 43, 44]. Gold nanorods (AuNRs) were obtained in two-step bottom-up *in situ* reactions using seed-mediated growth methods described by Nikoobakht *et al.* [43] with modifications [44, 45]. Gold seeds (seed solution) were prepared in the first step by dissolving CTAB surfactant (5 ml, 0.2 M) in deionized water, adding the $HAuCl_4$ precursor (5 ml, 0.0005 M), stirring for 10 min, and then adding the cooled reducing agent $NaBH_4$ (0.6 ml, 0.01 M) and vigorously stirring the mixture for 1.5 h. All reagents were added very quickly (one shot). $NaBH_4$ must be freshly prepared and added before bubbling appears, so we used water that had been frozen in an ice freezer in advance. The color of the mixture changed from yellow to brownish yellow. The seed solution was maintained at 28°C to prevent crystallization of the CTAB surfactant. The second step in the synthesis was the growth of gold seeds in solution (growth of nanorods in solution). Seed solution (12 µl) was added to the growth solution containing CTAB (5 ml, 0.2 M), $HAuCl_4$ (5 ml, 0.001 M), $AgNO_3$ (0.075 ml and 0.25 ml, 0.004 M), and ascorbic acid (0.07 ml, 0.078 M). The seed solution was added at a temperature of 27 to 30°C to allow the growth of the AuNRs. After adding the reducing agent to CTAB, the solution was stirred until it became a clear orange color.

PEG functionalization of AuNPs

The capping of AuNSs by PEG-SH (Mw ≈ 2000) followed the previously described protocol [46–48]. This process prevents aggregate formation and enhances nanoparticle stability. In brief, a small amount of previously sonicated PEG-SH (30 min at 40°C) was added to the nanoparticle solution. The solution was stirred for 24 h to facilitate the exchange of citrate ligands with PEG-SH. Excess PEG-SH was removed by centrifugation at 6000 rpm for approx. 30 min (twice). PEGylated nanoparticle fractions were then suspended in a saline solution and stored at 4°C.

The size and location of the AuNRs' LSPR were controlled by varying the amount of $AgNO_3$. Excess reactants were removed by double centrifugation (6000 rpm for 30 min). The PEG-SH coating was prepared using a modified method as described previously [49, 50]. An aqueous PEG-SH solution was sonicated for 30 min at 40°C and added to the vigorously stirred AuNP solution. The mixture was stirred for 24 h at room temperature to ensure complete ligand exchange with PEG-SH. The minimal amount of PEG-SH required to stabilize the surface of AuNRs was determined according to Manson *et al.* [51]. Unbound PEG-SH particles were then removed by centrifugation at 6000 rpm for 30 min, the supernatant was discarded, and the nanoparticles in the pellet were dispersed in Milli-Q water. After the second centrifugation, AuNRs were suspended in a saline solution.

Physicochemical characterization of AuNPs

The absorption spectra were obtained using a Varian Cary 4000 spectrometer. All measurements were performed at room temperature (Fig. 2).

Transmission electron microscope (TEM) images were taken with a JEOL 1400 microscope operating at 120 kV. AuNSs and AuNRs were drop-casted onto Cu grids and placed on a vacuum desiccator overnight (Fig. 3).

The electrokinetic potentials and size distributions of the AuNPs were measured using a Malvern Zetasizer Nano-ZS Dynamic Light Scattering Analyzer (Malvern Instruments Ltd.).

Isolation and culture of human lymphocytes

Peripheral blood mononuclear cells (PBMC) were isolated from buffy coat samples obtained at the local Blood

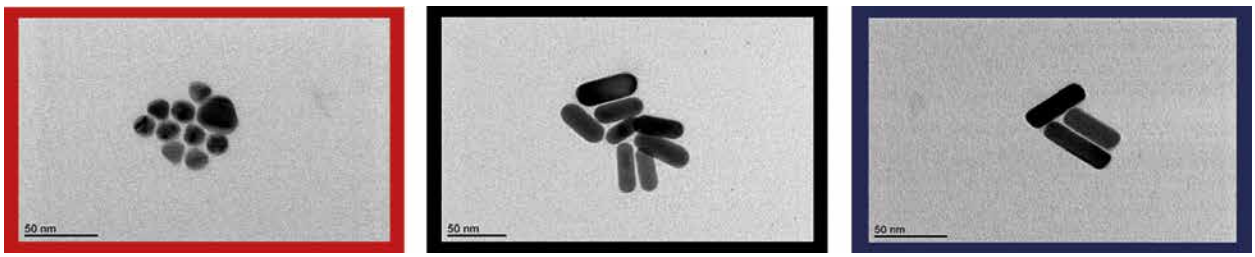

Fig. 3. TEM images of spherical gold nanospheres (AuNSs) and gold nanorods (AuNRs1 and AuNRs2). Colors correspond to those in Figure 2 (red, black, and blue, respectively)

Donation and Blood Treatment Center in Poznan, sourced from healthy volunteers, 8 males aged 29–49 years, who provided individual informed consent. The sodium citrate anticoagulated samples were diluted 1 : 6 in PBS containing heparin (3 mM). PBMCs were then isolated via density gradient centrifugation, using a lymphocyte separation medium (Sigma-Aldrich, C-44010), according to the manufacturer's instructions. Briefly, the cell suspension was carefully loaded on top of the separation medium, and then samples were centrifuged at 440 × g for 40 minutes at room temperature. The interphase of mononuclear cells was collected and washed twice with culture medium. Next, the cell pellet was resuspended in RPMI 1640 (Biowest L0500) supplemented with 10% (v/v) fetal bovine serum and 1% (v/v) penicillin-streptomycin solution and seeded onto a 96-well plate (2×10^5 cells/well).

Lymphocyte proliferation was stimulated with phytohemagglutinin (PHA-L; 2.5 µg/ml, MP Biomedicals, 151886). Cells were cultured for 72 h at 37°C in humidified air with 5% CO_2.

Evaluation of nanoparticle cytotoxicity

The PEGylated AuNSs had an average particle diameter of 15 nm, whereas the AuNRs were of two different sizes: AuNRs1: 20 × 40 nm and AuNRs2: 22 × 50 nm. All AuNPs were suspended in a physiological saline solution.

Working suspensions of PEGylated AuNPs were prepared from a 0.2 mg/ml stock to produce the desired final concentrations. One hundred microliters of AuNP suspension were added to the cultured lymphocytes at concentrations of 2, 4, 8, 16, 32, and 64 µg/ml. Each experiment used a vehicle control with pure physiological saline solution. Every sample was run in triplicate. The cells were incubated with the nanoparticles for 24 h. For the study design diagram see the supplementary figure.

Viability assessment

Cell viability was assessed using a 3-(4,5-dimethylthiazol-2-yl)-2,5-diphenyltetrazolium bromide (MTT) assay. In this method, metabolically active cells reduce MTT to an insoluble purple formazan via mitochondrial reductases. After solubilization, the formazan concentration was measured spectrophotometrically. The absorbance value was then used as an indicator of cellular viability [52, 53].

After the 24-h incubation with AuNPs, the cells were washed twice in RPMI 1640 without phenol red. Subsequently, MTT reagent (VWR Chemicals 0793, 1.2 mM) was added, and the plates were incubated for 4 h at 37°C. Following incubation, the formazan product was solubilized in DMSO, and the absorbance at 540 nm was measured using a microplate spectrophotometer (Epoch, BioTek Instruments, USA).

To correct for the absorbance originating from AuNPs remaining in the sample wells despite washing, cell-free

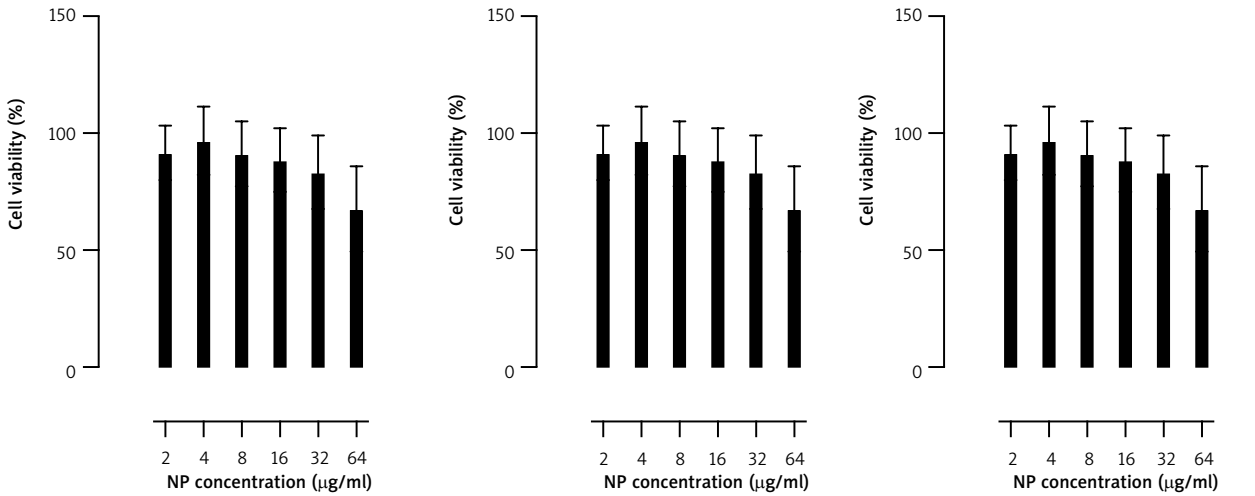

Fig. 4. Viability assessment of lymphocytes exposed for 24 h to different concentrations of AuNPs of three kinds: AuNSs (left); 15 nm, AuNRs1 (middle); 20 × 40 nm, AuNRs2 (right); 22 × 50 nm. Cell viability was evaluated using an MTT assay. $n = 8$, mean ± SD in three independent experiments. Numbers indicate p-values of the t-test for samples significantly different than the control ($p < 0.05$)

samples of AuNP suspensions at concentrations matching those used in the experiment were prepared and processed in the same manner as the experimental samples (washing, centrifugation, and incubations). The absorbance values of the AuNP samples at equivalent concentrations were then subtracted from the absorbance readings of the experimental samples (Fig. 4).

Cell viability was expressed as a percentage of the control, calculated using the following equation:

$$\text{Cell viability} = \frac{A_{treatment} - A_{blank}}{A_{ctrl} - A_{blank}} 100\%$$

Statistical analysis

The mean, standard deviation, median, and minimum and maximum values were calculated for all variables. Normality was assessed using the Shapiro-Wilk test. Statistical analysis was conducted using nonparametric methods because the assumptions for parametric tests were not met.

Changes in the viability of cells exposed to nanoparticles at increasing concentrations were assessed using Friedman's test. Samples exposed to different types of AuNPs at the same concentration were compared using the Kruskal-Wallis test. Post-hoc Dunn's test was applied in both cases to identify differing groups. Spearman's rank correlations were also used to explore possible relationships between nanoparticle concentration and cell viability.

For all calculations, a p-value<0.05 was considered statistically significant. The analyses were performed using Statistica software (version 13, TIBCO Software Inc., 2016).

Results

Synthesis and characterization of AuNPs

AuNSs and AuNRs were characterized using UV/vis spectroscopy and TEM (Fig. 3). The location of UV/vis bands provides information about the average particle size, whereas their full width at half maximum can be used to determine the dispersion of particles in a colloidal solution. The UV/vis extinction spectrum of AuNSs showed a characteristic single peak at 520 nm, whereas AuNRs exhibited both longitudinal and transverse LSPRs (Fig. 2). Spectroscopic studies in the UV/vis spectral range showed that the resonance maximum was approx. 520 nm in the transverse direction and, in the longitudinal direction, could be tuned from the visible to the near-infrared range, depending on the presence of $AgNO_3$ in the growth solution (the maximum was at 640 nm or 745 nm). The final concentration of AuNPs was calculated according to Fernández-López *et al*. [46]. The functionalization of AuNPs improves their stability in various solvents. PEG-SH was chosen not only for its biocompatibility and low cytotoxicity but also for its particularly strong affinity for AuNPs, facilitating binding by forming a gold-thiolate bond. All PEGylated AuNPs were prepared in three concentrations: 20, 100, and 200 µg/ml and then transferred to a saline solution (similar to human body fluids with 0.9% NaCl). The hydrodynamic diameter of the AuNSs was measured by dynamic light scattering. The size distribution of the AuNSs was 45 nm and 58 nm before and after functionalization, respectively. The zeta potentials of AuNSs changed from –12.1 mV to –21.3 mV after PEG functionalization. Naked AuNRs showed cationic surfaces 11.7 mV and 12.7 mV for AuNRs1 and AuNRs2, respectively. After functionalization the zeta potentials were reduced to negative levels (–16.0 mV – AuNRs1 and –18.7 mV – AuNRs2).

Cytotoxicity of AuNPs

In our experiments, AuNPs of all three sizes/shapes negatively affected the viability of activated human lymphocytes in a dose-dependent manner, with the highest concentration (64 µg/ml) causing the most significant decrease (Fig. 4). For AuNSs and AuNRs1, a significant decrease in viability was observed at concentrations of 32 and 64 µg/ml. Statistical analysis showed that the difference in effect between concentrations of 32 and 64 µg/ml was significant ($p < 0.05$) only for AuNSs. For AuNRs2, the effect of AuNPs at 8 µg/ml was significantly weaker than at 16 µg/ml ($p < 0.05$), 32 µg/ml, and 64 µg/ml ($p < 0.001$). The concentration of 16 µg/ml had a significantly weaker effect than 64 µg/ml ($p < 0.01$).

AuNRs2 decreased lymphocyte viability significantly more strongly than AuNRs1 at concentrations of 8, 16, and 32 µg/ml. At concentrations of 16, 32, and 64 µg/ml, AuNRs2 had a significantly stronger effect on lymphocyte viability than AuNSs. AuNRs1 affected lymphocyte viability significantly more strongly than AuNSs but only at a concentration of 64 µg/ml.

Overall, larger AuNRs (approx. 22 × 50 nm) were more toxic than smaller 20 × 40 nm AuNRs and 15 nm AuNSs, but the observed differences in the AuNP-induced reduction in lymphocyte viability were significant only at high concentrations.

Discussion

The literature describes the influence of various media on the stability of AuNPs (water, phosphate-buffered saline, phosphate-buffered saline containing bovine serum albumin, and dichloromethane) [51]. PEGylated AuNSs were also shown to be stable at salt concentrations ranging from 0.15 to 1 M [51], whereas citrate-capped AuNPs aggregated immediately. The PEG coating greatly improved the suspension stability in all tested media. Due to the NaCl, PEG-functionalized AuNSs showed lower stability after redispersion in phosphate-buffered saline and phosphate-buffered saline/bovine serum albumin, compared to dichloromethane and water [51]. Stiufiuc *et al*. [54] reported a fast and efficient one-step synthesis of AuNSs coated with unmodified PEG of various molecular weights and surface charges. The ligand exchange reaction is often used as a highly versatile tool to functionalize Au-NPs for specific applications. Removing surface-bound CTAB with more biocompatible surface ligands is required for biological applications of AuNPs. CTAB is cytotoxic; hence, PEG-SH is one of the most important ligands used for this purpose, because it confers superior biocompatibility and colloidal protection of PEG-S protected AuNPs. However, it was difficult to produce high-yield ligand exchange products that

effectively remove CTAB. During the ligand exchange reaction, the Au-S bond was created, and unbonded PEG was removed through centrifugation.

The results confirmed that the surface-enhanced Raman scattering signal is unaffected by the length of the PEG molecular chain enclosing the nanoparticle and that the stability is not affected by the addition of a strong salt solution (0.1 M NaCl), indicating its potential use for *in vitro* and *in vivo* applications.

Although AuNPs have various applications, particularly in humans, their use must overcome the impact of NaCl and pH. Therefore, Tseng *et al*. [55] incorporated NaCl into a pulse spark discharge system used for AuNP synthesis to simulate the human body and study its stability. The addition of a long-chain carboxymethylcellulose polymer or polyvinylpyrrolidone k30 (PVP-k30) has been shown to prevent aggregation and precipitation in NaCl or different pH values and maintain dispersion by increasing the repulsive force between particles. A similar observation in AuNRs showed that 1.0 M NaCl did not affect the tensile strength of PEGylated AuNRs, whereas CTAB-stabilized nanoparticles aggregated immediately upon the addition of NaCl [56]. Furthermore, the concentration of PEG and the functionalization process do not affect the optical properties of AuNPs.

The size-dependent cytotoxicity of AuNPs *in vitro* has been extensively researched, but some studies have produced conflicting results. AuNPs affect not only the viability but also the proliferation of lymphocytes. The apparent contradiction in experimental results is unsurprising because the dimensions and AR of AuNPs are just two among many factors that determine their uptake and toxicity. Parameters such as surface charge and ligand chemistry [31], the presence of residual chemicals, surface capping methods, and protein adsorption on AuNPs also affect the rate of internalization [32]. Both inhibitory and stimulatory effects of AuNPs on mitogen-stimulated lymphocyte proliferation have been reported. Liptrott *et al*. [57] demonstrated a concentration-dependent stimulatory effect of 8.8 nm AuNPs on PHA-stimulated PBMC proliferation. This effect was partially attenuated when the AuNPs were capped with a ligand shell. Conversely, Devanabanda *et al*. [58] observed dose-dependent inhibition of mitogen-stimulated (PHA or PWM) proliferation of lymphocytes incubated with 50 nm AuNPsClick or tap here to enter text. Mitogen-stimulated lymphocyte proliferation is typically assessed via [^{3}H]thymidine incorporation, which allows monitoring of the rate of DNA synthesis [58]. In assessing cell viability by MTT reduction, viability is inferred from the bulk activity of intracellular oxidoreductases and electron donors that reduce MTT to colored formazans. The result of the MTT reaction depends on both cellular metabolism and the number of cells in the sample [59, 60]. Therefore, in our experiments, to avoid confusing the potential stimulatory or antiproliferative effects of AuNPs with a decline in viability, AuNPs were added to the culture at 72 h after mitogen stimulation. We chose this timing because most lymphocytes are expected to have already entered the G1 stage of the cell cycle, and the effect of the nanoparticles on lymphocyte activation should be minimal [61, 62].

Devanabanda *et al*. [58] found that AuNPs with an average diameter of 50 nm had no effect on the viability of human and murine lymphocytes after 72 h of incubation at concentrations up to 200 µg/ml. However, the proliferative response to mitogens, including PHA, was inhibited in a dose-dependent manner. The AuNPs used in their study were not PEGylated and were synthesized through a chemical reduction method using trisodium citrate. Saqr *et al*. [63] found that 70-nm non-PEGylated AuNPs synthesized via a reduction method involving plant extracts were cytotoxic to HeLa and normal human primary osteoblasts at concentrations as low as 0.62 µg/ml. Abo-Zeid *et al*. [64] investigated the cytotoxicity of 50-nm and 30-nm PEGylated AuNRs, 15-nm AuNSs, as well as semicubes in human lymphocytes in the concentration range of 0.05 to 1 µg/ml. They observed an increase in cytotoxicity and inhibition of mitotic activity with decreasing AuNP size. Interestingly, Yu Pan *et al*. [65], in a study with ultrasmall, spherical, non-PEGylated, phenylphosphine-capped AuNPs, found a size difference as small as 0.2 nm to be relevant in terms of cytotoxicity. In HeLa cells, 1.2-nm AuNPs after 24 h of incubation were found to mainly cause apoptosis, whereas incubation with slightly larger 1.4 nm AuNPs resulted in a much higher percentage of necrotic cells in the annexin V/PI assay. As mentioned above, ultrasmall AuNPs can enter the cell nucleus, whereas larger AuNPs tend to accumulate in the cytoplasm; therefore, the mechanism of their toxicity may be different [33]. Nuclear penetration is associated with higher toxicity [66].

Because of a multitude of conditions potentially affecting the experimental results, it is difficult to draw general conclusions about the effect of AuNPs on cell viability based on the outcomes of individual studies. The apparent discrepancies may result from various factors and experimental parameters, apart from AuNP size and AR, which account for differences in cell viability. These factors and parameters include, but are not limited to, cell type [67], incubation time, method of viability assessment [68], size range, surface charge, modifications [69] and the presence of impurities related to the method of AuNP synthesis [22, 70]. The CTAB surfactant commonly used in AuNR synthesis, if not removed or overcoated, can be responsible for the cytotoxicity of AuNR suspensions [22]. It has been suggested that surface chemistry plays a much larger role in AuNPs' toxicity than their size and morphology [71, 72]. Viability assessment results also depend on culture conditions, such as serum protein concentration, which affects AuNPs' cellular uptake [73].

Our analysis revealed the high inter-individual variability in response to AuNP exposure. The cytotoxicity of AuNPs as a function of their size and/or shape has been previously studied in various cell types, including cells of epithelial origin: HEP-2 and canine MDCK [74], U87 and primary human dermal fibroblasts [20, 71, 75], HeLa and HEK293T [76], BEAS-2B cells (transformed human bronchial epithelial cells) [77], MCF-7 and SKBR-3 breast cancer cells, as well as PC-3 prostate cancer cells [69, 78], rat cardiomyocytes [79], HepG2 liver cancer cells and HL-7702

J774 normal liver cells [80], A549 and NCIH441 lung adenocarcinoma cells [70], A1 murine macrophages [81] and B lymphocytes [15]. Most of these studies were based on established continuous cell lines. This approach allows for high replicability; however, it might not accurately reflect individual susceptibility to the toxicity of AuNPs. Immortal, genetically altered cell lines have inherent limitations as a model of *in vivo* state. Assessment of cell viability using a primary culture of donor-derived cells has the potential to be more reliable in predicting AuNP toxicity, albeit at the expense of reproducibility and statistical power. In our study, we used buffy coat, which is a by-product of blood processing in a blood donation center not normally used for transfusion. This provides a convenient way to obtain a large volume of white blood cells. It also allows multiple tests to be performed on cells obtained from a single donor from a single blood draw, eliminating one potential source of inconsistency.

Le Guével *et al*. [82] reported that AuNPs at nontoxic concentrations induced changes in lymphocyte subpopulations. Dendritic cells pretreated with 12-nm AuNPs stabilized with glutathione and co-cultured with lymphocytes stimulate the proliferation of Th1 lymphocytes and $CD56^{bright}$ NK cells secreting IFN-Click or tap here to enter text. These results suggest that AuNPs at concentrations below the toxic threshold may indirectly shift the balance in Th subpopulations in favor of Th1 cells. Both T and B lymphocytes can internalize AuNPs through endocytosis; however, PEGylation has been shown to significantly reduce the uptake of AuNPs by B cells [15, 83]. As indicated earlier [84], AuNP studies in the context of their biomedical applications must take into account the potential adverse impact of AuNPs on the normal function of the immune system and how the immune response may change the effectiveness of AuNP-based therapeutic or imaging procedures [19].

Our study was limited by the relatively small number of samples. Additionally, the MTT assay detects mitochondrial reductase activity, which generally correlates well with the number of viable cells in culture. However, the assay does not distinguish between changes in metabolic activity and decreases in cell number due to apoptosis and/or necrosis. Further studies will be needed to determine the mechanisms responsible for the decline in cell viability, and to investigate the ability of AuNPs to induce cell death in proliferating cells. Future studies should include an analysis of cellular uptake and membrane adhesion of AuNPs. One of the challenges of cytotoxicity testing is the insufficient sensitivity of available methods. The MTT assay, which is well established and widely used, may not be sensitive enough to measure the cytotoxic effects of nanoparticles at low concentrations. It is crucial to note that the size-dependent toxicity of AuNPs *in vivo* is related to their tendency to accumulate in organs and is strongly associated with circulation time [85]. Smaller AuNPs tend to pass through the renal filtration system, whereas larger nanoparticles accumulate in tissues, leading to potentially harmful changes in non-target sites of the body [86]. The distribution of AuNPs across organs and tissues adds another layer of complexity that is not addressed in this *in vitro* study and will require a different experimental approach.

Conclusions

Our results indicate that high concentrations of AuNPs have a detrimental impact on lymphocyte viability *in vitro*. Specifically, the 22 × 50 nm AuNRs exhibit greater toxicity compared to the 20 × 40 nm AuNRs and 15 nm AuNSs. Thus, when determining a safe dosage of AuNPs for therapeutic or diagnostic purposes, it is crucial to consider not only the concentration but also the shape and size of the nanoparticles. In the context of designing targeted photodynamic and photothermal cancer therapies, it is essential to recognize the light-independent, non-selective cytotoxic effects of AuNPs on both tumor and normal cells. Therefore, current and future *in vivo* applications of AuNPs necessitate a careful evaluation of the benefits and risks associated with exposing living cells to nanomaterials. Achieving the right balance involves selecting the optimal size and surface modifications to minimize adverse effects while retaining the desired properties of AuNPs.

Disclosures

1. Institutional review board statement: This study was approved by the Bioethics Committee of Poznan University of Medical Sciences (approval number: KB 423/23).
2. Assistance with the article: The authors gratefully acknowledge Emerson Coy for the TEM images.
3. Financial support and sponsorship: This research was funded by the National Science Center in Poland under project 2021/41/N/ST4/03017 (to P.B.).
4. Conflicts of interest: None.

References

1. Jeong EH, Jung G, Hong CA, Lee H. Gold nanoparticle (AuNP)-based drug delivery and molecular imaging for biomedical applications. Arch Pharm Res 2014; 37: 53-59.
2. Venditti I. Engineered gold-based nanomaterials: morphologies and functionalities in biomedical applications. A mini review. Bioeng 2019; 6: 53.
3. Elahi N, Kamali M, Baghersad MH. Recent biomedical applications of gold nanoparticles: a review. Talanta 2018; 184: 537-556.
4. Cao J, Sun T, Grattan KTV. Gold nanorod-based localized surface plasmon resonance biosensors: a review. Sensors Actuators B Chem 2014; 195: 332-351.
5. Jain PK, Huang X, El-Sayed IH, El-Sayed MA. Noble metals on the nanoscale: optical and photothermal properties and some applications in imaging, sensing, biology, and medicine. Acc Chem Res 2008; 41: 1578-1586.
6. Pellas V, Hu D, Mazouzi Y, Mimoun Y, Blanchard J, Guibert C, et al. Gold nanorods for LSPR biosensing: synthesis, coating by silica, and bioanalytical applications. Biosensors 2020; 10: 146. DOI: 10.3390/bios10100146.
7. Youssef Z, Yesmurzayeva N, Larue L, Jouan-Hureaux V, Colombeau L, Arnoux P, et al. New targeted gold nanorods for the treatment of glioblastoma by photodynamic therapy. J Clin Med 2019; 8: 2205. DOI: 10.3390/jcm8122205.
8. Liao S, Yue W, Cai S, Tang Q, Lu W, Huang L, et al. Improvement of gold nanorods in photothermal therapy: recent progress and perspective. Front Pharmacol 2021; 12: 664123. DOI: 10.3389/fphar.2021.664123.
9. Marangoni VS, Bernardi JC, Reis IB, Fávaro WJ, Zucolotto V. Photothermia and activated drug release of natural cell membrane coated plasmonic gold nanorods and β-lapachone. ACS Appl Bio Mater 2019; 2: 728-736.

10. Overchuk M, Weersink RA, Wilson BC, Zheng G. Photodynamic and photothermal therapies: synergy opportunities for nanomedicine. ACS Nano 2023; 17: 7979-8003.
11. Błaszkiewicz P, Kotkowiak M. Gold-based nanoparticles systems in phototherapy – current strategies. Curr Med Chem 2018; 25: 5914-5929.
12. Suk JS, Xu Q, Kim N, Hanes J, Ensign LM. PEGylation as a strategy for improving nanoparticle-based drug and gene delivery. Adv Drug Deliver Rev 2016; 99 (Pt A): 28-51.
13. Kang H, Buchman JT, Rodriguez RS, Ring HL, He J, Bantz KC, et al. Stabilization of silver and gold nanoparticles: preservation and improvement of plasmonic functionalities. Chem Rev 2019; 119: 664-699.
14. Partikel K, Korte R, Stein NC, Mulac D, Herrmann FC, Humpf HU, et al. Effect of nanoparticle size and PEGylation on the protein corona of PLGA nanoparticles. Eur J Pharm Biopharm 2019; 141: 70-80.
15. Hočevar S, Milošević A, Rodriguez-Lorenzo L, Ackermann-Hirschi L, Mottas I, Petri-Fink A, et al. Polymer-coated gold nanospheres do not impair the innate immune function of human B lymphocytes in vitro. Acs Nano 2019; 13: 6790-6800.
16. Alkilany AM, Murphy CJ. Toxicity and cellular uptake of gold nanoparticles: what we have learned so far? J Nanopart Res 2010; 12: 2313-2333.
17. Sani A, Cao C, Cui D. Toxicity of gold nanoparticles (AuNPs): a review. Biochem Biophysics Rep 2021; 26: 100991. DOI: 10.1016/j.bbrep.2021.100991.
18. Enea M, Pereira E, Almeida MP de, Araújo AM, Bastos M de L, Carmo H. Gold nanoparticles induce oxidative stress and apoptosis in human kidney cells. Nanomaterials (Basel) 2020; 10: 995. DOI: 10.3390/nano10050995.
19. Gallud A, Klöditz K, Ytterberg J, Östberg N, Katayama S, Skoog T, et al. Cationic gold nanoparticles elicit mitochondrial dysfunction: a multi-omics study. Sci Rep 2019; 9: 4366. DOI: 10.1038/s41598-019-40579-6.
20. Mateo D, Morales P, Ávalos A, Haza AI. Comparative cytotoxicity evaluation of different size gold nanoparticles in human dermal fibroblasts. J Exp Nanosci 2015; 10: 1401-1417.
21. Mitarotonda R, Giorgi E, Eufrasio-da-Silva T, Dolatshahi-Pirouz A, Mishra YK, Khademhosseini A, et al. Immunotherapeutic nanoparticles: from autoimmune disease control to the development of vaccines. Biomaterials Adv 2022; 135: 212726-212726.
22. Alkilany AM, Nagaria PK, Hexel CR, Shaw TJ, Murphy CJ, Wyatt MD. Cellular uptake and cytotoxicity of gold nanorods: molecular origin of cytotoxicity and surface effects. Small 2009; 5: 701-708.
23. Zhao Y, Wang Y, Ran F, Cui Y, Liu C, Zhao Q, et al. A comparison between sphere and rod nanoparticles regarding their in vivo biological behavior and pharmacokinetics. Sci Rep 2017; 7: 4131.
24. Chithrani BD, Ghazani AA, Chan WCW. Determining the size and shape dependence of gold nanoparticle uptake into mammalian cells. Nano Lett 2006; 6: 662-668.
25. Yang K, Ma YQ. Computer simulation of the translocation of nanoparticles with different shapes across a lipid bilayer. Nat Nanotechnol 2010; 5: 579-583.
26. Gao H, Shi W, Freund LB. Mechanics of receptor-mediated endocytosis. Proc National Acad Sci 2005; 102: 9469-9474.
27. Gratton SEA, Ropp PA, Pohlhaus PD, Luft JC, Madden VJ, Napier ME, et al. The effect of particle design on cellular internalization pathways. Proc National Acad Sci 2008; 105: 11613-11618.
28. Huang X, Teng X, Chen D, Tang F, He J. The effect of the shape of mesoporous silica nanoparticles on cellular uptake and cell function. Biomaterials 2010; 31: 438-448.
29. Kolhar P, Anselmo AC, Gupta V, Pant K, Prabhakarpandian B, Ruoslahti E, et al. Using shape effects to target antibody-coated nanoparticles to lung and brain endothelium. Proc National Acad Sci 2013; 110: 10753-10758.
30. Arnida, Malugin A, Ghandehari H. Cellular uptake and toxicity of gold nanoparticles in prostate cancer cells: a comparative study of rods and spheres. J Appl Toxicol 2010; 30: 212-217.
31. Lin J, Miao L, Zhong G, Lin CH, Dargazangy R, Alexander-Katz A. Understanding the synergistic effect of physicochemical properties of nanoparticles and their cellular entry pathways. Commun Biol 2020; 3: 205. DOI: 10.1038/s42003-020-0917-1.
32. Lesniak A, Salvati A, Santos-Martinez MJ, Radomski MW, Dawson KA, Åberg C. Nanoparticle adhesion to the cell membrane and its effect on nanoparticle uptake efficiency. J Am Chem Soc 2013; 135: 1438-1444.
33. Huang K, Ma H, Liu J, Huo S, Kumar A, Wei T, et al. Size-dependent localization and penetration of ultrasmall gold nanoparticles in cancer cells, multicellular spheroids, and tumors in vivo. ACS Nano 2012; 6: 4483-4493.
34. Oh E, Delehanty JB, Sapsford KE, Susumu K, Goswami R, Blanco-Canosa JB, et al. Cellular uptake and fate of pegylated gold nanoparticles is dependent on both cell-penetration peptides and particle size. ACS Nano 2011; 5: 6434-6448.
35. Palombo M, Deshmukh M, Myers D, Gao J, Szekely Z, Sinko PJ. Pharmaceutical and toxicological properties of engineered nanomaterials for drug delivery. Annu Rev Pharmacol 2012; 54: 581-598.
36. Chen YS, Hung YC, Liau I, Huang GS. Assessment of the in vivo toxicity of gold nanoparticles. Nanoscale Res Lett 2009; 4: 858-864.
37. Qiu Y, Liu Y, Wang L, Xu L, Bai R, Ji Y, et al. Surface chemistry and aspect ratio mediated cellular uptake of Au nanorods. Biomaterials 2010; 31: 7606-7619.
38. Kinnear C, Rodriguez-Lorenzo L, Clift MJD, Goris B, Bals S, Rothen-Rutishauser B, et al. Decoupling the shape parameter to assess gold nanorod uptake by mammalian cells. Nanoscale 2016; 8: 16416-16426.
39. Zhang XD, Wu D, Shen X, Liu PX, Yang N, Zhao B, et al. Size-dependent in vivo toxicity of PEG-coated gold nanoparticles. Int J Nanomed 2011; 6: 2071-2081.
40. Macintyre AN, Rathmell JC. Activated lymphocytes as a metabolic model for carcinogenesis. Cancer Metab 2013; 1: 5. DOI: 10.1186/2049-3002-1-5.
41. Błaszkiewicz P, Kotkowiak M, Dudkowiak A. Fluorescence quenching and energy transfer in a system of hybrid laser dye and functionalized gold nanoparticles. J Lumin 2017; 183: 303-310.
42. Talarska P, Błaszkiewicz P, Kostrzewa A, Wirstlein P, Cegłowski M, Nowaczyk G, et al. Effects of spherical and rod-like gold nanoparticles on the reactivity of human peripheral blood leukocytes. Antioxidants 2024; 13: 157. DOI: 10.3390/antiox13020157.
43. Nikoobakht B, El-Sayed MA. Preparation and growth mechanism of gold nanorods (NRs) using seed-mediated growth method. Chem Mater 2003; 15: 1957-1962.
44. Błaszkiewicz P, Kotkowiak M, Coy E, Dudkowiak A. Laser-induced optoacoustic spectroscopy studies of inorganic functionalized metallic nanorods. J Phys Chem C 2019; 123: 27181-27186.
45. Błaszkiewicz P, Kotkowiak M, Coy E, Dudkowiak A. Tailoring fluorescence and singlet oxygen generation of a chlorophyll derivative and gold nanorods via a silica shell. J Phys Chem C 2020; 124: 2088-2095.
46. Fernández-López C, Mateo-Mateo C, Álvarez-Puebla RA, Pérez-Juste J, Pastoriza-Santos I, Liz-Marz'an LM. Highly controlled silica coating of PEG-capped metal nanoparticles and preparation of SERS-encoded particles. Langmuir 2009; 25: 13894-13899.
47. Rahme K, Chen L, Hobbs RG, Morris MA, O'Driscoll C, Holmes JD. PEGylated gold nanoparticles: polymer quantification as a function of PEG lengths and nanoparticle dimensions. Rsc Adv 2013; 3: 6085-6094.
48. Shimmin RG, Schoch AB, Braun PV. Polymer size and concentration effects on the size of gold nanoparticles capped by polymeric thiols. Langmuir 2004; 20: 5613-5620.
49. Szustakiewicz P, Kołsut N, Leniart A, Lewandowski W. Universal method for producing reduced graphene oxide/gold nanoparticles composites with controlled density of grafting and long-term stability. Nanomaterials (Basel) 2019; 9: 602. DOI: 10.3390/nano9040602.
50. Tim B, Błaszkiewicz P, Nowicka AB, Kotkowiak M. Optimizing SERS performance through aggregation of gold nanorods in Langmuir-Blodgett films. Appl Surf Sci 2022; 573: 151518. DOI: https://doi.org/10.1016/j.apsusc.2021.151518.
51. Manson J, Kumar D, Meenan BJ, Dixon D. Polyethylene glycol functionalized gold nanoparticles: the influence of capping density on stability in various media. Gold Bull 2011; 44: 99-105.

52. Kumar P, Nagarajan A, Uchil PD. Analysis of cell viability by the MTT assay. Cold Spring Harb Protoc 2018; 2018: pdb.prot095505. DOI: 10.1101/pdb.prot095505.
53. Mosmann T. Rapid colorimetric assay for cellular growth and survival: application to proliferation and cytotoxicity assays. J Immunol Methods 1983; 65: 55-63.
54. Stiufiuc R, Iacovita C, Nicoara R, Stiufiuc G, Florea A, Achim M, et al. One-step synthesis of PEGylated gold nanoparticles with tunable surface charge. J Nanomater 2013; 2013. DOI: https://doi.org/10.1155/2013/146031.
55. Tseng KH, Hsieh CL, Huang JC, Tien DC. The effect of NaCl/pH on colloidal nanogold produced by pulsed spark discharge. J Nanomater 2015; 2015. DOI: 10.1155/2015/612324.
56. Zhang Z, Lin M. Fast loading of PEG–SH on CTAB-protected gold nanorods. RSC Adv 2014; 4: 17760-17767.
57. Liptrott NJ, Kendall E, Nieves DJ, Farrell J, Rannard S, Fernig DG, et al. Partial mitigation of gold nanoparticle interactions with human lymphocytes by surface functionalization with a mixed matrix. Nanomedicine (Lond) 2014; 9: 2467-2479.
58. Devanabanda M, Latheef SA, Madduri R. Immunotoxic effects of gold and silver nanoparticles: Inhibition of mitogen-induced proliferative responses and viability of human and murine lymphocytes in vitro. J Immunotoxicol 2016; 13: 397-902.
59. Stepanenko AA, Dmitrenko VV. Pitfalls of the MTT assay: direct and off-target effects of inhibitors can result in over/underestimation of cell viability. Gene 2015; 574: 193-203.
60. Berridge MV, Herst PM, Tan AS. Tetrazolium dyes as tools in cell biology: new insights into their cellular reduction. Biotechnology Annu Rev 2005; 11: 127-152.
61. Kotecki M, Pawlak AL, Wiktorowicz KE. The inhibitory effect of theophylline on cell cycle kinetics of human lymphocytes in vitro. Arch Immunol Ther Exp (Warsz) 1989; 37: 725-733.
62. Takase K, Terada N, Lucas JJ, Gelfand EW. Control of cell cycle entry and progression in mitogen-stimulated human B lymphocytes. J Cell Physiol 1995; 162: 246-255.
63. Saqr AA, Khafagy ES, Alalaiwe A, Aldawsari MF, Alshahrani SM, Anwer MdK, et al. Synthesis of gold nanoparticles by using green machinery: characterization and in vitro toxicity. Nanomaterials (Basel) 2021; 11: 808. DOI: 10.3390/nano11030808.
64. Abo-Zeid MAM, Liehr T, Gamal-Eldeen AM, Zawrah M, Ali M, Othman MAK. Potential of rod, sphere and semi-cube shaped gold nanoparticles to induce cytotoxicity and genotoxicity in human blood lymphocytes in vitro. Eur J Nanomed 2015; 7. DOI: https://doi.org/10.1515/ejnm-2014-0031.
65. Pan Y, Neuss S, Leifert A, Fischler M, Wen F, Simon U, et al. Size-dependent cytotoxicity of gold nanoparticles. Small 2007; 3: 1941-1949.
66. Magogotya M, Vetten M, Roux-van der Merwe MP, Badenhorst J, Gulumian M. In vitro toxicity and internalization of gold nanoparticles (AuNPs) in human epithelial colorectal adenocarcinoma (Caco-2) cells and the human skin keratinocyte (HaCaT) cells. Mutat Res Genetic Toxicol Environ Mutagen 2022; 883: 503556. DOI: 10.1016/j.mrgentox.2022.503556.
67. Chueh PJ, Liang RY, Lee YH, Zeng ZM, Chuang SM. Differential cytotoxic effects of gold nanoparticles in different mammalian cell lines. J Hazard Mater 2014; 264: 303-312.
68. Steckiewicz KP, Barcinska E, Malankowska A, Zauszkiewicz-Pawlak A, Nowaczyk G, Zaleska-Medynska A, et al. Impact of gold nanoparticles shape on their cytotoxicity against human osteoblast and osteosarcoma in in vitro model. Evaluation of the safety of use and anti-cancer potential. J Mater Sci Mater Med 2019; 30: 22. DOI: 10.1007/s10856-019-6221-2.
69. Vijayakumar S, Ganesan S. In vitro cytotoxicity assay on gold nanoparticles with different stabilizing agents. J Nanomater 2012; 2012. DOI: https://doi.org/10.1155/2012/734398.
70. Uboldi C, Bonacchi D, Lorenzi G, Hermanns MI, Pohl C, Baldi G, et al. Gold nanoparticles induce cytotoxicity in the alveolar type-II cell lines A549 and NCIH441. Part Fibre Toxicol 2009; 6: 18. DOI: 10.1186/1743-8977-6-18.
71. Bhamidipati M, Fabris L. Multiparametric assessment of gold nanoparticle cytotoxicity in cancerous and healthy cells: the role of size, shape, and surface chemistry. Bioconjugate Chem 2017; 28: 449-460.
72. Alkilany AM, Thompson LB, Boulos SP, Sisco PN, Murphy CJ. Gold nanorods: their potential for photothermal therapeutics and drug delivery, tempered by the complexity of their biological interactions. Adv Drug Deliver Rev 2012; 64: 190-199.
73. Carnovale C, Bryant G, Shukla R, Bansal V. Identifying trends in gold nanoparticle toxicity and uptake: size, shape, capping ligand, and biological corona. ACS Omega 2019; 4: 242-256.
74. Zhang Y, Xu D, Li W, Yu J, Chen Y. Effect of size, shape, and surface modification on cytotoxicity of gold nanoparticles to human HEp-2 and canine MDCK cells. J Nanomater 2012; 2012. DOI: https://doi.org/10.1155/2012/375496.
75. Mironava T, Hadjiargyrou M, Simon M, Jurukovski V, Rafailovich MH. Gold nanoparticles cellular toxicity and recovery: effect of size, concentration and exposure time. Nanotoxicology 2010; 4: 120-137.
76. Woźniak A, Malankowska A, Nowaczyk G, Grześkowiak BF, Tuśnio K, Słomski R, et al. Size and shape-dependent cytotoxicity profile of gold nanoparticles for biomedical applications. J Mater Sci Mater Med 2017; 28: 92. DOI: 10.1007/s10856-017-5902-y.
77. Vales G, Suhonen S, Siivola KM, Savolainen KM, Catalán J, Norppa H. Genotoxicity and cytotoxicity of gold nanoparticles in vitro: role of surface functionalization and particle size. Nanomaterials (Basel) 2020; 10: 271. DOI: 10.3390/nano10020271.
78. White BE, White MK, Alsudani ZAN, Watanabe F, Biris AS, Ali N. Cellular uptake of gold nanorods in breast cancer cell lines. Nanomaterials (Basel) 2022; 12: 937. DOI: 10.3390/nano12060937.
79. Henson JC, Brickell A, Kim JW, Jensen H, Mehta JL, Jensen M, et al. PEGylated gold nanoparticle toxicity in cardiomyocytes: assessment of size, concentration, and time dependency. IEEE Trans Nanobioscience 2022; 21: 387-394.
80. Wang P, Wu Q, Wang F, Zhang Y, Tong L, Jiang T, et al. Evaluating cellular uptake of gold nanoparticles in HL-7702 and HepG2 cells for plasmonic photothermal therapy. Nanomedicine (Lond) 2018; 13: 2245-2259.
81. Yen H, Hsu S, Tsai C. Cytotoxicity and immunological response of gold and silver nanoparticles of different sizes. Small 2009; 5: 1553-1561.
82. Le Guével X, Palomares F, Torres MJ, Blanca M, Fernandez TD, Mayorga C. Nanoparticle size influences the proliferative responses of lymphocyte subpopulations. Rsc Adv 2015; 5: 85305-85309.
83. Zupke O, Distler E, Jrchott A, Paiphansiri U, Dass M, Thomas S, et al. Nanoparticles and antigen-specific T-cell therapeutics: a comprehensive study on uptake and release. Nanomedicine 2015; 10: 1063-1076.
84. Zhu GH, Azharuddin M, Islam R, Rahmoune H, Deb S, Kanji U, et al. Innate immune invisible ultrasmall gold nanoparticles – framework for synthesis and evaluation. Acs Appl Mater Inter 2021; 13: 23410-23422.
85. Ajnai G, Chiu A, Kan T, Cheng CC, Tsai TH, Chang J. Trends of gold nanoparticle-based drug delivery system in cancer therapy. J Exp Clin Med 2014; 6: 172-178.
86. Vines JB, Yoon JH, Ryu NE, Lim DJ, Park H. Gold nanoparticles for photothermal cancer therapy. Front Chem 2019; 7: 167. DOI: 10.3389/fchem.2019.00167.

Address for correspondence

Jacek Sikora, PhD
Department of Immunobiology
Poznan University of Medical Sciences
8 Rokietnicka St.
60-806 Poznan, Poland
e-mail: jmsikora@ump.edu.pl

Submitted: 11.09.2024
Accepted: 28.10.2024